HHS Public Access

Author manuscript

Phys Rev Lett. Author manuscript; available in PMC 2021 January 17.

Published in final edited form as:

Phys Rev Lett. 2020 January 17; 124(2): 027801. doi:10.1103/PhysRevLett.124.027801.

Topological Linking Drives Anomalous Thickening of Ring Polymers In Weak Extensional Flows

Thomas C. O'Connor[1,*], **Ting Ge**[2], **Michael Rubinstein**[2], **Gary S. Grest**[1]

[1]Sandia National Laboratories, Albuquerque, New Mexico, 87185, USA

[2]Department of Mechanical Engineering and Materials Science, Duke University, Durham, North Carolina, 27708, USA

Abstract

Molecular dynamics simulations confirm recent extensional flow experiments showing ring polymer melts exhibit strong extension-rate thickening of the viscosity at Weissenberg numbers $Wi \ll 1$. Thickening coincides with the extreme elongation of a minority population of rings that grows with Wi. The large susceptibility of some rings to extend is due to a flow-driven formation of topological links that connect multiple rings into supramolecular chains. Links form spontaneously with a longer delay at lower Wi and are pulled tight and stabilized by the flow. Once linked, these composite objects experience larger drag forces than individual rings, driving their strong elongation. The fraction of linked rings depends non-monotonically on Wi, increasing to a maximum when $Wi \sim 1$ before rapidly decreasing when the strain rate approaches $1/\tau_e$.

Non-concatenated ring polymers do not entangle like linear polymers, and they tend to have lower Newtonian viscosities than linear melts of similar molecular weight [1–6]. However, recent experiments by Huang et al. [7] show that ring melts are extraordinarily sensitive to extensional flow, exhibiting large, nonlinear growth in the extensional viscosity η_{ex} even when the strain rate $\dot{\epsilon}$ is small compared to the reciprocal ring relaxation time $1/\tau_{ring}$ in equilibrium. Such trends are usually due to polymer conformations elongating in the flow field [5, 8–11], but analytic and numerical models for linear response predict this shouldn't happen when $\dot{\epsilon} \ll 1/\tau_{ring}$ [5, 6].Thus, it appears that new physics emerges and changes how rings dissipate energy in uniaxial extensional flows.

Huang et al. observed an apparent correspondence between the high-rate extensional viscosity η_{ex} of ring and linear melts of Polystyrene (PS) with the same $M_w = 185$ kg/mol, leading them to propose that rings transition to behaving like linear chains as they elongate [7]. However, prior simulation studies of unentangled ring and linear melts under planar extension did not observe a clear correspondence at large Wi [12]. In addition, scaling arguments and simulations of linear melts predict that η_{ex} should scale as $\sim N^2$ for linear chains near full extension. [9] and as $\sim N^2/4$ for rings if they behave like linear chains. Thus, extended rings of N monomers should behave like linear chains with $N/2$ monomers, but this was not observed in experiments.

* toconno@sandia.gov.

Here, we use MD simulations to show that the unintuitive rheology of rings under uniaxial extension is driven by a new topological linking mechanism that assembles rings into supramolecular daisy-chains during flow (Fig. 1). We simulate start-up uniaxial extensional flows for ring and linear polymer melts at several molecular weights. Simulations reproduce the strong sensitivity of rings to uniaxial extension reported by Huang et al., and also reveal qualitative differences between the elongation dynamics of rings and linear chains. While chains in linear melts elongate independently during extension, the susceptibility of rings to assemble into supramolecules can drive a minority of rings to elongate and dominate the nonlinear viscosity, even when $W_i \ll 1$. While many quantum materials in applied magnetic fields develop topological interactions that drive nonlinear response, ring polymers linking during extension is the first instance of a similar effect in a classical polymer liquid.

We model polymers with a standard semi-flexible bead-spring model that has been used to study ring melts in equilibrium and under shear [8, 13]. All beads interact with a truncated Lennard-Jones (LJ) potential and results are presented in reduced LJ units. Rings of N = 200, 400, and 800 beads are bound together with a FENE potential with mean bond length b ≈ 0.96. The chain stiffness is controlled by a bond bending potential $k_\theta(1-\cos\theta)$, where θ is the angle between successive bonds. In this study, we fix k_θ = 1.5, which gives a Kuhn segment length $n_K \sim 2.88$ beads and an entanglement strand containing $N_e \approx 28$ beads [14].

M ring or linear polymers of length N are equilibrated at a temperature T = 1 and density ρ = 0.85 using the methods detailed in Ref. 15 and Ref. 4, respectively. Rings are allowed to diffuse for ~ $10\,\tau_{\text{ring}}$ prior to elongation. The majority of our analysis considers a ring melt with M = 5000 and N = 400 ($Z = N/N_e \approx 14$) that most closely correspond to the experimental results of Huang et al. on polystyrene (PS) of M_w = 185 kg/mol [7]. In order to compare trends for different molecular weights and compare rings to linear melts, we also model ring melts with: M = 200, N = 200; M = 5000, N = 800; and linear melts with M = 1640, N = 112; M = 250, N = 200; M = 400, N = 400. All simulations are performed using LAMMPS with a time-step Δt = 0.007.

Melts are elongated at constant Hencky strain rate $\dot{\varepsilon} \equiv \partial \ln \Lambda / \partial t$ with Λ the stretch along the z-axis. Upper limits of $\dot{\varepsilon}$ are chosen to avoid covalent bond stretching. Since polymers are nearly incompressible, the two perpendicular directions contract uniformly to preserve volume. Generalized Kraynik-Reinelt boundary conditions are used to prevent the simulation box from collapsing in the contracting directions [9, 16–18]. Flow is maintained by integrating the G-SLLOD equations of motion with a thermostat damping time of 10 [19, 20]. Like experiments, we record the start-up extensional viscosity $\eta_{\text{ex}}(t) = \sigma_{\text{ex}}/\dot{\varepsilon}$ during flow, where the extensional stress $\sigma_{\text{ex}} = \sigma_{zz} - \sigma_{rr}$ is the difference in stress between the extension axis (z-axis) and the transverse directions.

Experiments typically analyze data from different chemistries by comparing them in reduced units derived from linear response. The same approach can be used to compare bead-spring simulations to the experiments of Huang et al. [7] For bead-spring simulations, $\tau_{\text{ring}}(N)$ is taken from Ge and Rubinstein's fits of simulation data to the Fractal-Loopy-Globule (FLG) model[6]. For the experiments, we use the empirically measured τ_{ring} = 52.6 s. Strain rates

are reported as a dimensionless Weissenberg number $Wi = \dot{\varepsilon}\tau$, with $\tau = \tau_{\text{ring}}$ for rings and $\tau = \tau_R = \tau_e Z^2$ for linear melts. τ_R is the Rouse time which is the longest dissipative relaxation time of a linear chain in the absence of entanglements. It can be related to the entanglement time τ_e and the number of entanglements per chain Z. Prior studies on this bead-spring model have measured $\tau_e \approx 1.98 \times 10^3$ [14].

Figure 2 plots the normalized extensional viscosity $\eta_{\text{ex}}/\eta_{\text{ex}}^N$ versus reduced time t/τ_{ring} for a bead-spring melt of rings alongside the experimental curves from Huang et al. [7]. Simulation data are smoothed over time with a Gaussian kernel. Both simulation and experiment use rings with $Z \sim 14$. η_{ex}^N is the Newtonian viscosity taken from the plateau of the linear viscoelastic envelope (LVE). The experimental LVE is take from Ref. 7, while the simulated LVE is taken from Eq. 49 of Ref. 6.

The simulations reproduce the qualitative trends with Wi that are seen in experiments. Both show a large nonlinear growth in η_{ex} above the Newtonian viscosity even for $Wi \ll 1$. Extraordinarily, even for the lowest $Wi = 0.17$, thickening above η_{ex}^N is observed in simulations after $\sim 30\,\tau_{\text{ring}}$. As there is no uncertainty about the homogeneity of composition or flow in the simulated melts, our data support Huang et al.'s conclusion that ring melts exhibit an anomalously large (and seemingly delayed) sensitivity to extensional flow.

Comparing the experimental curves to simulations in Figure 2 shows an apparent difference in the trend of terminal viscosity with Wi. Simulations resolve steady-state plateaus in η_{ex} for $Wi > 0.17$ that are a factor ~ 10 larger than η_{ex}^N and that weakly decrease with increasing Wi. In contrast, experiments, particularly at lower Wi, do not resolve clear plateaus and give terminal viscosities that decrease towards η_{ex}^N as Wi decreases. These differences appear to be due to different maximum strains in simulations and experiments. The average maximum strain in the experiments is $\varepsilon \sim 5$, while our ring simulations all reach $\varepsilon > 12$. The simulation curves are marked with an "X" at the points corresponding to $\varepsilon = 5$. Simulations truncated at $\varepsilon = 5$ show the same qualitative trends with Wi as seen in experiments. This suggests that the ring experiments at low Wi are likely not resolving steady-state viscosities, so comparing these values to steady-state η_{ex} for linear melts is difficult. Further, due to the apparent instability of rings towards thickening at times $t > > \tau_{\text{ring}}$, current experiments may not be able to reach sufficiently large strains to resolve steady-states at low Wi.

Figure 3 compares steady-state η_{ex} versus $\dot{\varepsilon}$ for three ring and three linear molecular weights. For the smallest $N = 200$ rings and $N = 112$ linears, the steady η_{ex} converge once $\dot{\varepsilon} > 10^{-4}$. However, this correspondence disappears with increasing molecular weight N. $N = 400$ rings and $N = 200$ linears show a similar decrease in η_{ex} with increasing $\dot{\varepsilon}$, but ring η_{ex} are consistently $\sim 2 - 3$ times larger until $\dot{\varepsilon} > 2 \times 10^{-4}$. At higher rates, the linear melt stops thinning while η_{ex} for rings continue to decrease. $N = 800$ rings and $N = 400$ linears exhibit similar behavior, however, the separation between ring and linear η_{ex} at intermediate rates has grown to a factor $\sim 4 - 5$.

Prior studies found $\eta_{ex} \sim N^2$ for linear chains at large Wi [9], the rings do not follow this scaling over our range of $\dot{\varepsilon}$. Thus, the viscosity of an elongated melt of N-rings is not simply related to that of an elongated linear melt. The ring-linear correspondence observed by Huang et al. for PS with $Z \sim 14$ may be a crossing of two different N dependencies at large Wi, like our 200-ring and 112-linear data appear to be.

The different trends in η_{ex} in Figure 3 imply that rings and linear chains are governed by different physics in extensional flows. This becomes clear when we examine the conformations of chains during flow. A common measure of linear chain elongation is the rms-magnitude of the end-end vector $\vec{R}$ connecting the two chain ends. Rings do not have chain ends, so instead we define an effective end-end distance for a ring as the maximum distance spanned by any pair of monomers on the ring that are separated by $N/2$ bonds. With this definition, an N-ring at full extension has approximately the same R as an (N/2)-linear chain.

Figure 4 shows steady-state span distribution functions $P(R)$ at three values of Wi for N = 400 rings (solid lines) and N = 200 linear chains (dashed lines). The Wi for the ring and linear chains are approximately the same for the three cases. For linear melts, $P(R)$ exhibits a narrow distribution that shifts to larger R with increasing Wi. This is consistent with the assumption that a deformed entanglement network transmits macroscopic strains independently to each chain. However, the distributions for rings exhibit a fundamentally different behavior. At the low Wi = 0.3, $P(R)$ for the rings develop a long tail corresponding to a small number of highly stretched rings. The tail grows with increasing Wi, producing a broad distribution for $Wi \sim 1$. For $Wi >> 1$, the flow becomes fast enough to elongate all rings and $P(R)$ narrows to a single peak centered at large R.

At low Wi the fraction of highly elongated rings is small, but their contribution to the extensional stress is substantial. This is due to the nonlinear increase in the entropic tension of a ring with increasing R. If we approximate the elongated rings to be under uniform tension, we can estimate the nonlinear increase in entropic tension as $\propto \mathscr{L}^{-1}(h)h$, where $\mathscr{L}^{-1}$ is the inverse Langevin function and $h = R/(bN/2)$ is the extension ratio of the ring. In Figure 4, the relative contribution of the rings to the stress $\propto P(R)\mathscr{L}^{-1}(h)h$ is plotted with a dotted line. For Wi = 27, the distributions for rings and linears are similar and all rings contribute substantially to the stress. However, as Wi decreases, the stress contributions become increasingly dominated by the small number of highly elongated rings. This is fundamentally different from linear melts and unprecedented for monodisperse polymers. While linear melt structure can be described with average conformational statistics, outliers dominate the non-linear response of rings.

MD simulations provide the microscopic details necessary to identify the physics driving the strong extension of some rings at low Wi. Rings are susceptible to linking with each-other to form "reef" or "lark's head" knots, shown in Figure 1(e). These are formed when a ring that has threaded another ring then threads back through itself, as in Figure 1(d). We observe that these links can form when chains are still in compact globular conformations. However,

once linked, rings form supramolecules with effectively higher molecular weights and relaxation times, becoming more susceptible to elongation.

We directly observe tight-links in steady-state simulations by applying primitive path analysis (PPA) to our MD trajectories [21]. Adapting techniques from prior ring studies [5, 6], we take a snapshot of the system and fix the coordinates of a single bead on each ring that is closest to the ring's geometric center. Intramolecular repulsive interactions are then removed, driving rings to collapse into points unless they are topologically linked. Collapsed rings have radii of gyration $R_g \sim 1$, much smaller than the average $R_g^{\mathrm{eq}} \approx 7.14$ in equilibrium. We measure an upper bound ϕ_{top} for the fraction of topologically linked rings by eliminating any ring that collapses to $R_g < 0.5 R_g^{\mathrm{eq}} < 3.57$, which is significantly smaller than the smallest ring conformations observed in equilibrium. While not a direct count of link numbers, this protocol identifies the fraction of chains participating in elongated clusters that are mediated by links (Fig. 1(a)&(b)) and that contribute significantly to the stress.

Figure 1(a) shows several highly elongated clusters of rings from the terminal state of the lowest $Wi = 0.17$ flow. Figure 1(b) shows the same rings after PPA, revealing many tight-links connecting rings into supramolecules. Figure 1(c) shows a close up of a tight-link between two rings before (left) and after (right) PPA. A supplemental video shows the spontaneous linking of three rings in a $Wi = 0.42$ flow[22]. Notably, links can form spontaneously during flow between rings that were far apart prior to startup. In addition, supramolecules are not limited to single links, with Figure 1(a) and (b) showing supramolecules of 6, 5, and 3 rings. In fact, we expect nonlinear response to be dominated by larger supramolecules at $Wi = 0.17$, since they must be be large enough to be pulled tight by low strain rate. The long delay in thickening at low Wi could be due to a long induction time for larger supramolecules to develop.

The effective relaxation times of supramolecules in flow should be significantly larger than for individual rings. Every linked chain adds N monomers to a supramolecule, and we would expect the effective Rouse time of q linked molecules to scale as $\sim q^2$. Thus, linked rings experience a much larger drag in flow than unlinked rings at the same $\dot{\epsilon}$, leading to their strong extension. Once elongated, links are pulled tight into reef knots (Figure 1(c)), stabilizing them for as long as flow persists. The ring topology is also important for stabilizing links. Unlike the recently observed transient hooking of rings by linear chains [11], ring-ring links cannot be destroyed by convective-constraint release because rings lack ends.

Figure 5(a) plots the fraction of topologically linked rings ϕ_{top} at the terminal strain for all Wi of the $N = 400$ melt. $\phi_{\mathrm{top}} \sim 0.005$ at $Wi = 0.17$ and increases with increasing Wi up to $\phi_{\mathrm{top}} \sim 0.20$ for $Wi > 1$. This persists until $Wi > 50$, where ϕ_{top} rapidly decreases to < 0.01. The sudden decrease at $Wi \approx 50$ corresponds to $\dot{\epsilon}\tau_e \approx 0.75$, with $\dot{\epsilon}$ approaching the reciprocal of the fundamental loop relaxation time [6]. These trends further imply the existence of an induction time for rings to sample threaded conformations that can form links. Once $\dot{\epsilon}\tau_e \sim 1$, we expect rings elongate faster than they can sample such link-forming configurations.

Following previous studies [9], we can approximate an entropic extensional stress σ_{ent} contributed by elongated rings:

$$\sigma_{ent} = \frac{\rho k_B T}{n_k}\left\langle \frac{2R}{Nb}\mathcal{L}^{-1}\left(\frac{2R}{Nb}\right)P_2\right\rangle \quad (1)$$

Here, ρ is the monomer density, n_k is the Kuhn segment length of the chains and P_2 is the nematic orientational order parameter for the ring span $\vec{R}$ relative to the extension axis. O'Connor et al. [9] found that Eq. 1 applied to entanglement segments in linear melts predicted the steady σ_{ex} for a wide range of Wi. Figure 5(b) compares σ_{top} to σ_{ex} for the terminal state of the $N = 400$ ring melt for all Wi. The entropic prediction closely follows σ_{ex} and agrees especially well at large Wi, as $P(R)$ (Figure 4) becomes a narrow distribution. Deviations are maximum 30–40% at $Wi = 0.17$; however, this Wi has not reached a steady-state, so $P(R)$ and σ_{ent} are not yet well defined.

The population ϕ_{top} drives the nonlinear rise in σ_{ex} at low Wi. This is seen by measuring the entropic stress contributed by just the topologically linked rings σ_{top} by only including the ϕ_{top} population in the expectation value of Eq. 1. The fraction $\sigma_{top}/\sigma_{ent}$ is shown as circles in Figure 5(a). Consistent with Figure 4, the decreasing fraction ϕ_{top} of linked rings contributes increasingly to the stress as Wi becomes small. Indeed, at $Wi = 0.17$, linked chains comprising less than 0.5% of the system contribute ~ 75% of σ_{top}. In other words, supramolecules contribute most of the anomalous stress observed at low Wi. $\sigma_{top}/\sigma_{ent}$ decreases with increasing Wi as ϕ_{top} saturates and then rapidly decreases. Unlinked rings also elongate and contribute substantially to the stress at as Wi increases, further reducing $\sigma_{top}/\sigma_{ent}$.

To conclude, MD simulations reproduce the experimental sensitivity of ring melts to extensional flows. Anomalous increases of η_{ex} at low Wi are caused by a fraction ϕ_{top} of rings that PPA reveals are topological linking to form supramolecular daisy-chains that elongate at lower Wi than single rings. Microscopic measures of ring entropy directly relate the nonlinear rise in stress to these elongated supramolecules. Unlike the transient "hooking" of rings by linear chains [11], these new ringring links are pulled tight and stabilized by the flow. Thus, supramolecules can persist even if Wi is changed. Our future efforts will study the dynamics of topological link formation during transient flow and stress relaxation. This will require adapting new ring analysis methods [23, 24] to accurately identify and track links as they form.

Supplementary Material

Refer to Web version on PubMed Central for supplementary material.

ACKNOWLEDGMENTS

M. R. acknowledges financial support from National Science Foundation under Grant No. EFMA-1830957, the National Institutes of Health under Grant Nos. P01HL108808, R01-HL136961, and 5UH3HL123645, and the Cystic Fibrosis Foundation. This work was supported by the Sandia Laboratory Directed Research and Development Program. This work was performed, in part, at the Center for Integrated Nanotechnologies, an Office

of Science User Facility operated for the U.S. Department of Energy (DOE) Office of Science. Sandia National Laboratories is a multi-mission laboratory managed and operated by National Technology & Engineering Solutions of Sandia, LLC, a wholly owned subsidiary of Honeywell International, Inc., for the U.S. DOEs National Nuclear Security Administration under contract DE-NA-0003525. The views expressed in the article do not necessarily represent the views of the U.S. DOE or the United States Government.

References

[1]. Rubinstein M, Dynamics of ring polymers in the presence of fixed obstacles, Phys. Rev. Lett 57, 3023 (1986). [PubMed: 10033934]

[2]. Obukhov SP, Rubinstein M, and Duke T, Dynamics of a Ring Polymer in a Gel, Phys. Rev. Lett 73, 1263 (1994). [PubMed: 10057666]

[3]. Kapnistos M, Lang M, Vlassopoulos D, PyckhoutHintzen W, Richter D, Cho D, Chang T, and Rubinstein M, Unexpected power-law stress relaxation of entangled ring polymers, Nature Materials 7, 997 (2008). [PubMed: 18953345]

[4]. Halverson JD, Lee WB, Grest GS, Grosberg YA, and Kremer K, Molecular dynamics simulation study of nonconcatenated ring polymers in a melt: I. statics, J. Chem. Phys 134, 204904 (2011).

[5]. Halverson JD, Lee WB, Grest GS, Grosberg YA, and Kremer K, Molecular dynamics simulation study of nonconcatenated ring polymers in a melt: Ii. dynamics, J. Chem. Phys 134, 204905 (2011).

[6]. Ge T, Panyukov S, and Rubinstein M, Self-Similar Conformations and Dynamics in Entangled Melts and Solutions of Nonconcatenated Ring Polymers, Macromolecules 49, 708 (2016). [PubMed: 27057066]

[7]. Huang Q, Ahn J, Parisi D, Chang T, Hassager O, Panyukov S, Rubinstein M, and Vlassopoulos D, Unexpected Stretching of Entangled Ring Macromolecules, Phys. Rev. Lett 122, 208001 (2019).

[8]. Halverson JD, Grest GS, Grosberg AY, and Kremer K, Rheology of ring polymer melts: From linear contaminants to ring-linear blends, Phys. Rev. Lett 108, 038301 (2012).

[9]. O'Connor TC, Alvarez NJ, and Robbins MO, Relating chain conformations to extensional stress in entangled polymer melts, Phys. Rev. Lett 121, 047801 (2018).

[10]. Mortensen K, Borger AL, Kirkensgaard JJ, Garvey CJ, Almdal K, Dorokhin A, Huang Q, and Hassager O, Structural Studies of Three-Arm Star Block Copolymers Exposed to Extreme Stretch Suggests a Persistent Polymer Tube, Phys. Rev. Lett 120, 207801 (2018).

[11]. Zhou Y, Hsiao K.-w., Regan KE, Kong D, Mckenna GB, Robertson-anderson RM, and Schroeder CM, dynamics in semidilute linear polymer solutions, Nature Communications, 1 (2019).

[12]. Yoon J, Kim J, and Baig C, Nonequilibrium molecular dynamics study of ring polymer melts under shear and elongation flows: A comparison with their linear analogs, Journal of Rheology 60, 673 (2016).

[13]. Kremer K and Grest GS, Dynamics of entangled linear polymer melts: A molecular-dynamics simulation, J. Chem. Phys 92, 5057 (1990).

[14]. Moreira LA, Zhang G, Müller F, Stuehn T, and Kremer K, Direct equilibration and characterization of polymer melts for computer simulations, Macromol. Theory Simul. 24, 419 (2015).

[15]. Auhl R, Everaers R, Grest GS, Kremer K, and Plimpton SJ, Equilibration of long chain polymer melts in computer simulations, J. Chem. Phys 119, 12718 (2003).

[16]. Dobson M, Periodic boundary conditions for long-time nonequilibrium molecular dynamics simulations of incompressible flows, J. Chem. Phys 141, 184103 (2014), arXiv:1408.7078.

[17]. Nicholson DA and Rutledge GC, Molecular simulation of flow-enhanced nucleation in n-eicosane melts under steady shear and uniaxial extension, J. Chem. Phys 145, 244903 (2016).

[18]. O'Connor TC, Hopkins A, and Robbins MO, Stress relaxation in highly oriented melts of entangled polymers, Macromolecules (Accepted Sept. 2019).

[19]. Evans DJ and Morriss GP, Nonlinear-response theory for steady planar couette flow, Phys. Rev. A 30, 1528 (1984).

[20]. Daivis PJ and Todd BD, A simple, direct derivation and proof of the validity of the sllod equations of motion for generalized homogeneous flows, J. Chem. Phys 124, 194103 (2006).

[21]. Everaers R, Sukumaran SK, Grest GS, Svaneborg C, Sivasubramanian A, and Kremer K, Rheology and Microscopic Topology of Entangled Polymeric Liquids, Science 303, 823 (2004). [PubMed: 14764875]

[22]. See Supplemental Material at [URL] for a video of three rings linking during the Wi = 0.42 flow.

[23]. Smrek J, Kremer K, and Rosa A, Threading of Unconcatenated Ring Polymers at High Concentrations: Double-Folded vs Time-Equilibrated Structures, ACS Macro Letters 8, 155 (2019). [PubMed: 30800531]

[24]. Schram RD, Rosa A, and Everaers R, Local loop opening in untangled ring polymer melts: a detailed Feynman test of models for the large scale structure, Soft Matter 15, 2418 (2019). [PubMed: 30778466]

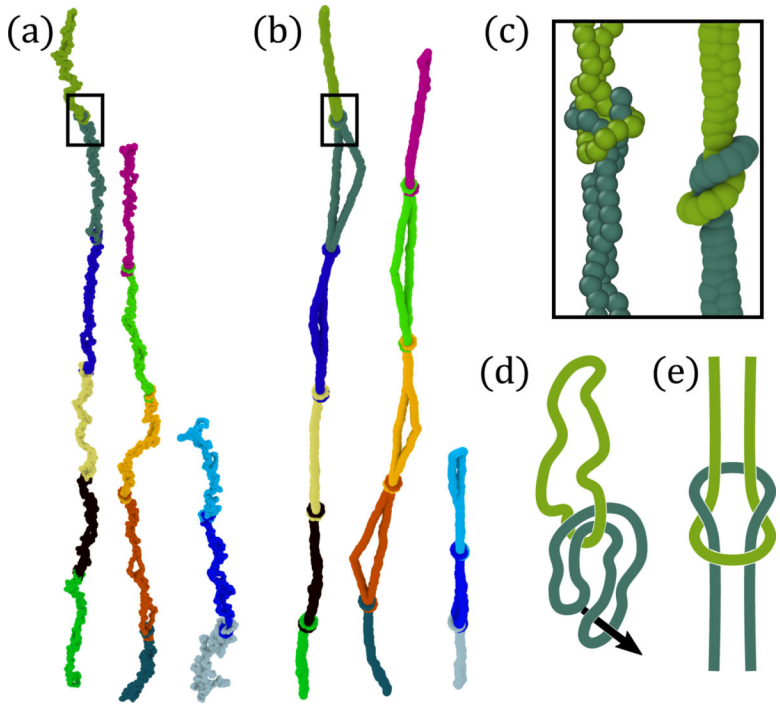

FIG. 1.

(a) Elongated $N = 400$ rings from the terminal state of the $Wi = 0.17$ flow. (b) Chains from (a) after PPA, revealing tight-links connecting rings into supramolecules. (c) Close-up of a tight-link framed in (a) and (b) before and after PPA. (d) Diagram of the formation of a link and (e) the final structure once it is pulled taut.

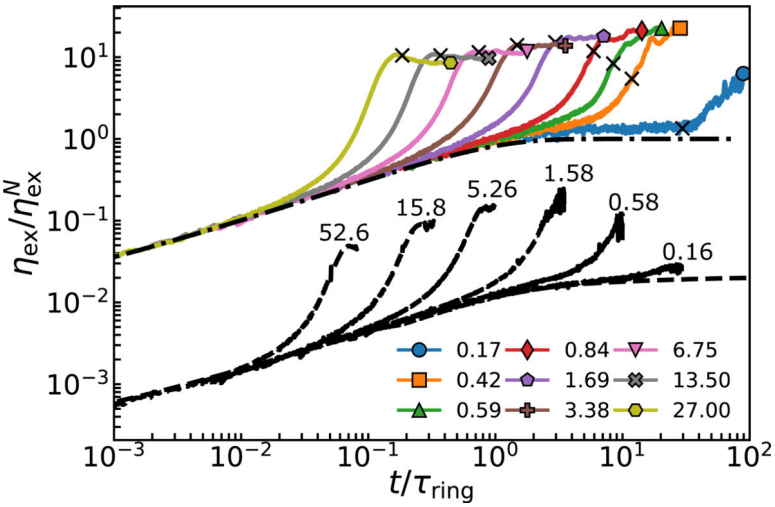

FIG. 2.

Start-up extensional viscosity η_{ex}/η_{ex}^N versus t/τ_{ring} for a N=400 ring melt (upper data) and PS experiments of Huang et al. [7] (lower data) at the indicated *Wi*. Dashed and dot-dashed lines show linear envelopes for experiments and simulations, respectively. Both simulations and experiments are for $Z \approx 14$ and experiments are shifted down by a factor of 100 for clarity. Experiments terminate at lower Hencky strains ($\varepsilon \sim 5$) then simulations (> 12). Crosses on simulated curves indicate $\varepsilon = 5$.

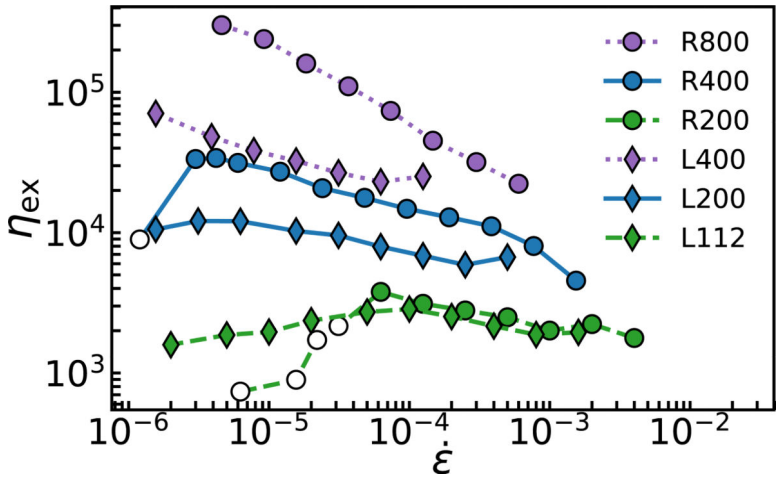

FIG. 3.

Steady-state η_{ex} versus $\dot{\varepsilon}$ for all three ring molecular weights compared to linear melt data with $N_l \approx N/2$. N_l are chosen so elongated rings and linears have similar dimensions at full extension. Unfilled symbols are points that did not reach steady-state by $\varepsilon = 12$.

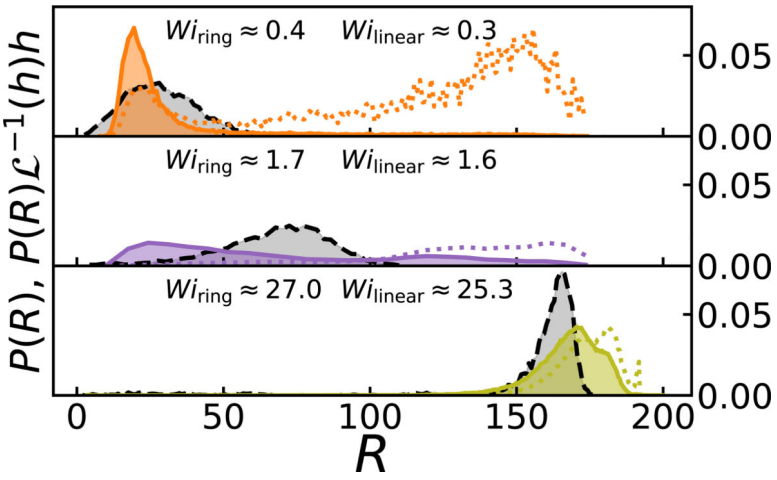

FIG. 4.

Steady-state $P(R)$ for $N = 400$ rings (solid) and $N = 200$ linears (dashed) at three Wi. Relative stress contributions $P(R)\mathscr{L}^{-1}(h)h$ for rings (dotted) are scaled to fit on the same axes.

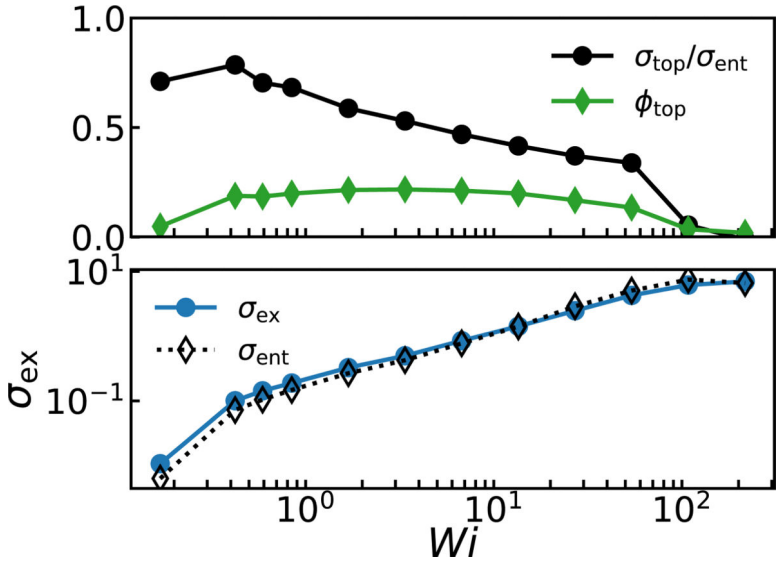

FIG. 5.

(a) Fraction of topologically linked rings ϕ_{top} and fraction of the entropic stress $\sigma_{top}/\sigma_{ent}$ they contribute versus Wi for $N = 400$ rings. (b) Steady-state stress σ_{ex} versus Wi compared to σ_{ent} from Eq. 1 for an $N = 400$ ring melt.